Correlating Reaction Dynamics and Size Change during the Photomechanical Transformation of 9-Methylanthracene Single Crystals

Kohei Morimoto, Daichi Kitagawa, Fei Tong, Kevin Chalek, Leonard J. Mueller, Christopher J. Bardeen, Seiya Kobatake

Correlating Reaction Dynamics and Size Change During the Photomechanical Transformation of 9-Methylanthracene Single Crystals

Kohei Morimoto[a], Daichi Kitagawa*[a], Fei Tong[b], Kevin Chalek[b], Leonard J. Mueller[b], Christopher J. Bardeen*[b], and Seiya Kobatake*[a]

[a]Department of Applied Chemistry
Graduate School of Engineering, Osaka City University,
3-3-138 Sugimoto. Sumiyoshi-ku
Osaka, 558-8585 (Japan)

[b]Department of Chemistry
University of California, Riverside
501 Big Springs Road
Riverside, CA 92521 (USA)

*E-mail: kitagawa@osaka-cu.ac.jp; christopher.bardeen@ucr.edu; kobatake@a-chem.eng.osaka-cu.ac.jp

Abstract

Photomechanical molecular crystals that expand under illumination could potentially be used as photon-powered actuators. In this study, we find that the use of high-quality single crystals of 9-methylanthracene leads to more homogeneous reaction kinetics than that previously seen for polycrystalline samples, presumably due to a lower concentration of defects. Furthermore, simultaneous observation of absorbance and shape changes in single crystals revealed that the dimensional change mirrors the reaction progress, resulting in a smooth expansion of 7% along the *c*-axis that is linearly correlated with reaction progress. The same expansion dynamics are highly reproducible across different single crystal samples. Organic single crystals exhibit well-defined linear expansions during 100% photoconversion, suggesting that this class of solid-state phase change material could be used for actuation.

Introduction

The ability of organic molecules to undergo large geometry changes during isomerization reactions and then maintain their new shapes after the photons are removed, makes them ideal elements for photon-powered actuation.[1,2] In order to translate molecular-level isomerization events into macroscopic motions, it is usually necessary to organize the photochromic molecules in some way. This organization can be accomplished using an ordered matrix like a polymer or liquid crystal. Alternatively, the molecules can be allowed to self-assemble by themselves into a crystal. Recent work has shown that molecular crystals are far from the fragile, static structures assumed by most chemists, exhibiting a variety of interesting mechanical properties.[3] Photomechanical molecular crystals can undergo a variety of light induced motions (bending,[4–8] twisting,[9,10] coiling,[11] peeling,[12–14] and hopping[15,16]) that are driven by a wide range of photochemical reactions, including cis-trans isomerizations, ring opening-closing isomerizations, linkage isomerizations, and [2+2] and [4+4] photodimerizations.

In most cases, the dramatic shape deformations of organic photomechanical structures result from partial reactant → product conversion that leads to the simultaneous presence of reactant and product domains.[17–19] The material then bends to accommodate the internal strain at the interface. This bimorph or bimetal mechanism is the most common origin of photomechanical motion in both polymers and crystals. To maximize the work output, however, it would be desirable to achieve 100% reactant → product transformation, analogous to inorganic phase change materials like shape-memory alloys.[20,21] In this approach, the difference in size and orientation between the reactant and product phases leads to a change in crystal dimensions and a longitudinal displacement. Piezoelectric actuators based on longitudinal displacements can generate forces several orders of magnitude higher than those based on bending, suggesting that this approach could lead to higher performance in organic photomechanical materials.

In order to go beyond bimorph-based bending crystals, several challenges must be addressed. First, to 100% convert an optically dense crystal, the photoproduct must not absorb the excitation light in order to avoid a photostationary state and allow the photons to reach reactant molecules throughout the entire crystal. In practice, this requires a "negative" photochromic reaction in which the product absorption is shifted to higher energies than that of the reactant.[22,23] However, even if this photophysical requirement is fulfilled, there remain a number of other potential obstacles for using a crystal as a linear actuator that shows expansion/contraction along a specific direction. Crystal-to-crystal variations in defect density and morphology could result in a wide variation in behaviors and fracture susceptibility.[24–27] Partial reaction may lead to internal strain and bending, due to the bimorph effect described above. An actuator that bends as it expands would likely fall out of alignment.

The dynamics of the transition from the reactant to product also play a key role. Photochemical kinetics in solid-state samples, usually measured in bulk powders using nuclear magnetic resonance[28] or X-ray diffraction[29], can be very nonlinear, with sigmoidal decay curves that indicate auto-inhibition or auto-catalysis. Complex kinetics could lead to complex mechanical dynamics. For example, when organic crystals undergo temperature dependent transitions between polymorphic forms, the transitions can occur in two possible ways.[30–33] In the homogeneous nucleation mechanism, the product forms in small nuclei distributed uniformly throughout the crystal. As the reaction progresses, the nuclei grow and merge, and the entire crystal transforms homogeneously (at least on optical lengthscales) into the product phase. In the martensitic mechanism, on the other hand, a random incubation period precedes the sudden transformation to product as a reaction front sweeps across the crystal. Microscopic imaging of the propagating phase fronts and their acoustic signatures have provided experimental confirmation of thermal

martensitic transformations in organic crystals.[21,34–36] Despite some debate during the early days of solid-state photochemistry[37,38], there seems to be no clear consensus on whether a martensitic transition can be driven by a nonthermal, photochemical mechanism.

From the standpoint of making a practical actuator, the ideal situation is one where the crystal expansion proceeds smoothly with a simple relation between reaction progress and extension. Establishing this relation requires simultaneous measurement of both quantities, which is now possible thanks to the advances in crystal growth and preparation reported in this paper. We use the [4+4] photocycloaddition reaction of 9-methylanthracene (**9MA**) shown in Scheme 1 as a model system. The dimerization reaction destroys the conjugation of the anthracene ring and shifts the absorbance from ~400 nm down to ~280 nm, making it a classic case of negative photochromism. The **9MA** dimerization can be partially reversed by heating or 254 nm light,[39-41] but under ambient conditions the reaction is effectively irreversible, allowing the crystal product to be characterized. The ability to reproducibly grow ultrathin **9MA** crystals with well-defined crystallographic orientations that are weakly adhered to the substrate allows us to observe crystal expansion without the bimorph-induced bending and curling motions that obscure dimensional changes. We utilize microscopic measurements that correlate changes in absorption, fluorescence, birefringence, and crystal size. Surprisingly, we find significantly different photodimerization kinetics for single crystals versus polycrystalline films. We develop a nonlinear kinetic model, based on the Finke-Watzky formalism, that can describe both cases. High quality single crystals are much closer to the simple first-order kinetic limit, suggesting that structural defects in crystal powders may be partially responsible for nonlinear kinetic behavior. Furthermore, the ability to simultaneously observe photochemical and dimensional changes in well-defined single crystals allows us to make a quantitative connection between reaction kinetics and crystal expansion. We

find no evidence for a martensitic transformation – the transformation appears to occur in a homogeneous, continuous fashion to produce a new crystalline dimer polymorph. The predictable and robust kinetic and mechanical behavior of **9MA** single crystals suggests that there is no fundamental barrier to their application as light-driven phase change actuators. This detailed characterization of a photochemical phase transition that drives the mechanical expansion of a single crystal should provide a benchmark for future studies of photomechanical crystals.

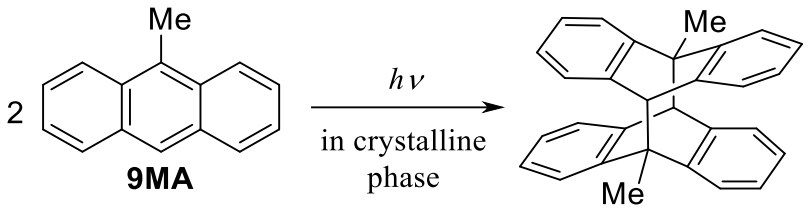

Scheme 1. Photodimerization reaction of 9-methylanthracene (**9MA**) in crystalline phase.

Results and Discussion

Crystal Morphology.

9MA thin crystals were prepared by the seeded-growth method reported previously.[42] The hexagonal top surface of the crystal was identified as the (100) and ($\bar{1}$00) surface with a space group of $P2_1/c$.[43] Figure 1 shows optical microphotograph of **9MA** single crystals, along with the crystal shape, and the molecular packing viewed from the flat face. When freely suspended in liquid, these crystals coil and uncoil when exposed to UV light which creates a monomer-dimer bimorph in the crystal.[42] To prevent these motions, we used two strategies to mount the crystals. At first, gentle evaporation of water on a glass surface resulted in crystals that adhered to the glass via a surfactant layer. These crystals could expand but could not delaminate from the glass surface. In order to completely avoid adhesion issues, we also made wet samples consisting of crystals still suspended in their growth solution and sandwiched between two glass plates. This sample has the advantage that the surrounding water should rapidly remove any heat build-up. Both approaches gave similar results, suggesting that weak surface adhesion and thermal effects play a negligible role in the expansion dynamics of the dry crystals.

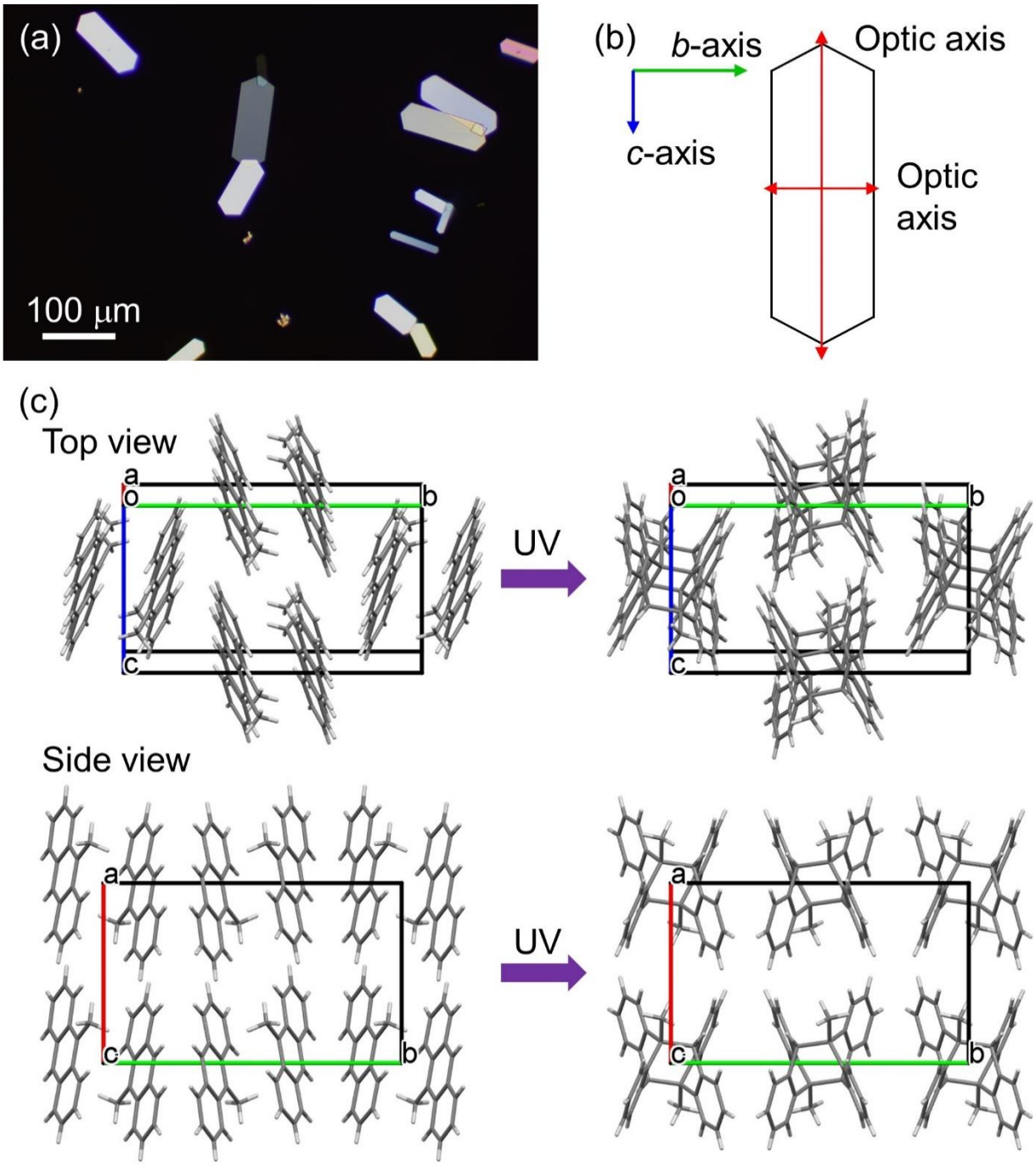

Figure 1. (a) Microphotograph of thin **9MA** crystals made by seeded-growth method under crossed Nicols, (b) crystal shape, and (c) crystal packing viewed from the observed surface ($\bar{1}00$) (Top view) and the cross-sectional view (Side view) before and after UV irradiation.

Reaction Kinetics in Single Crystal and Polycrystalline Film.

Previous experiments have measured the **9MA** photodimerization kinetics in polycrystalline samples, finding highly nonexponential behavior.[44] Here we directly measured the time-dependent monomer concentration using absorption spectroscopy in both single crystals and polycrystalline films. As for the single crystals, the polarized absorption spectrum was used to evaluate monomer concentration as a function of photoirradiation time. To avoid interference originating from birefringence, the spectra were measured perpendicular to the long axis of the crystal along the optic axis as shown in Figure 2a. Figure 2b shows the polarized absorption spectral change. The absorption peak of the monomer around 400 nm decayed upon UV (405 nm) irradiation and completely disappeared within about 200 seconds, suggesting that the crystal completed the photoreaction from the monomer to the dimer without fracture in crystals with thicknesses of 1 μm or less. The absorbance change shown in Figure 2c shows some sigmoidal character, but it is less pronounced than in a thin polycrystalline film prepared by casting the THF solution containing **9MA**, which is compared in Figure 2d.

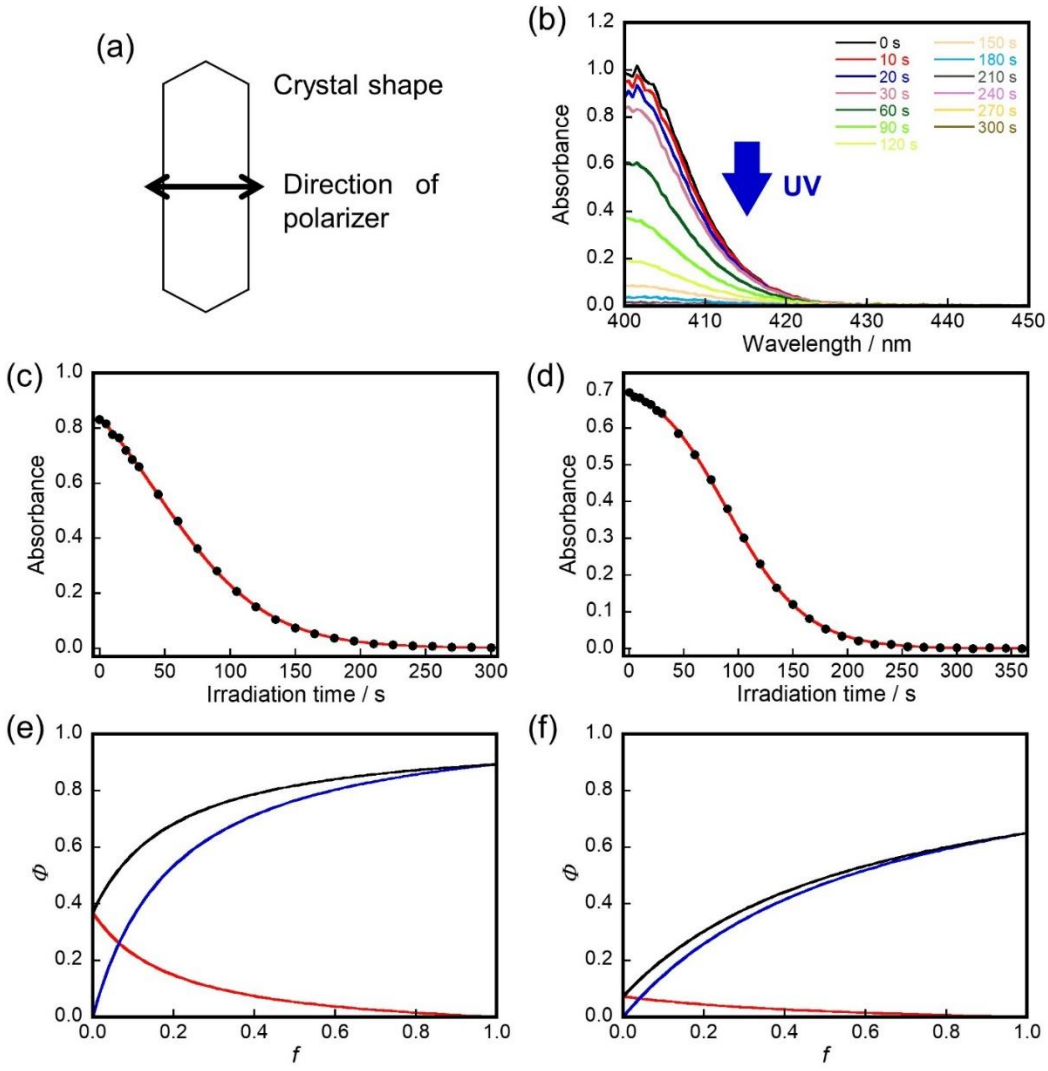

Figure 2. (a) The direction of polarizer for the extinction and the detection in single crystal, (b) the absorption spectral change (sample 1) upon polarized 405 nm light with 2.0×10^{15} photons cm^{-2} s^{-1} (= 0.98 mW cm^{-2}), (c) the experimental decay (black dots) at 405 nm of sample 1 and the fitting (red line) by Equation (5), (d) the experimental decay (black dots) at 405 nm of sample 4 upon nonpolarized 405 nm light with 1.5×10^{15} photons cm^{-2} s^{-1} (= 0.73 mW cm^{-2}) and the fitting (red line) by Equation (5), and (e, f) the quantum yield (Φ_1 (red), Φ_2 (blue), and Φ_{1+2} (black)) of samples 1 and 4. Note that the results setting $\sigma = 3.0\times10^{-17}$ cm^2 $molecule^{-1}$ were shown in (d, f).

The difference in kinetics between single crystal and polycrystalline film was surprising. In order to quantify the divergent behavior, we turned to a kinetic scheme based on a photophysical Finke-Watzky model.[44] If A represents the monomer pair and B the photodimer, we have the reaction scheme

$$A \xrightarrow{\sigma I} A^* \quad (1a)$$

$$A^* \xrightarrow{k_{ex}} A \quad (1b)$$

$$A^* + A \xrightarrow{k_1} B + A \quad (1c)$$

$$A^* + B \xrightarrow{k_2} B + B \quad (1d)$$

where σ is the absorption cross section at the excitation wavelength (cm^2 $molecule^{-1}$), I is the monochromatic light intensity for the photoreaction (photons cm^{-2} s^{-1}), k_{ex} is the relaxation rate constant of A to the ground state (s^{-1}). k_1 and k_2 are the rate constant (nm^3 $molecule^{-1}$ s^{-1}) of the reaction which is affected by A and B, respectively. We can derive three rate equations,

$$\frac{d[A]}{dt} = -\sigma I[A] + k_{ex}[A^*] \quad (2a)$$

$$\frac{d[A^*]}{dt} = +\sigma I[A] - k_{ex}[A^*] - k_1[A^*][A] - k_2[A^*][B] \quad (2b)$$

$$\frac{d[B]}{dt} = +k_1[A^*][A] + k_2[A^*][B] \quad (2c)$$

where [A] and [B] are the concentration (molecule nm^{-3}) of A and B. With Equations (2) and the relation $[B] = [A]_0 - [A]$, where $[A]_0$ is the initial monomer pair concentration, we can derive an equation that describes the time-dependent change in [A] as shown in Supporting Information:

$$\frac{d[A]}{dt} = -\sigma I[A]\left(\frac{\frac{[A]}{[A]_0} + \beta\left(1 - \frac{[A]}{[A]_0}\right)}{\alpha + \frac{[A]}{[A]_0} + \beta\left(1 - \frac{[A]}{[A]_0}\right)}\right) \quad (3)$$

where $\alpha = \frac{k_{ex}}{k_1[\mathrm{A}]_0}$ and $\beta = \frac{k_2}{k_1}$. β determines whether the chemical identity of its neighbor affects the reaction rate of A: $\beta = 1$ means that the rates are equal, while $\beta < 1$ means that A is less likely to react if it has a neighboring B, and $\beta > 1$ means that it is more likely to react (auto-catalysis). In the case of $\beta = 1$, Equation (3) yields a standard single exponential decay, while $\beta > 1$ yields a sigmoidal curve.

As [A] decreases, the light intensity I inside the crystal increases, so both I and [A] change with time. We can take this into account by scaling the measured intensity I_0 by the photokinetic factor F,

$$I = FI_0 = \frac{1-10^{-Abs}}{\ln(10)\,Abs} I_0 \tag{4}$$

where Abs is the monomer absorbance at the excitation wavelength. From the Lambert-Beer equation, [A] and $[\mathrm{A}]_0$ can be written as $Abs/\varepsilon l$ and $Abs_0/\varepsilon l$ where Abs_0 is the initial absorbance at the excitation wavelength, ε is the molecular absorption coefficient for the monomer pair, and l is the crystal thickness. Combining Equations (3) and (4), we arrive at an equation to fit the measured $Abs(t)$ curves:

$$\frac{\mathrm{d}Abs}{\mathrm{d}t} = -\frac{\sigma I_0}{\ln(10)}(1-10^{-Abs})\left(\frac{\frac{Abs}{Abs_0} + \beta\left(1-\frac{Abs}{Abs_0}\right)}{\alpha + \frac{Abs}{Abs_0} + \beta\left(1-\frac{Abs}{Abs_0}\right)}\right) \tag{5}$$

Fitting the data using Equation (5) yields the constants α and β, but in order to make the results interpretable using standard photochemistry concepts, we define effective quantum yields for the k_1 and k_2 photochemical reaction pathways as follow,

$$\Phi_1 = \frac{k_1[A]}{k_{ex} + k_1[A] + k_2[B]} = \frac{1-f}{\alpha + 1 - f + \beta f} \tag{6a}$$

$$\Phi_2 = \frac{k_2[B]}{k_{ex} + k_1[A] + k_2[B]} = \frac{\beta f}{\alpha + 1 - f + \beta f} \quad (6b)$$

where $f = \frac{[A]_0 - [A]}{[A]_0} = \frac{[B]}{[A]_0}$ is the fraction of crystal converted to photodimer. It turns out that Φ_1 and Φ_2 are not constant but depend on the dimer fraction *f*. The total of the quantum yield Φ_{1+2} related to the photoreaction is defined by,

$$\Phi_{1+2} = \Phi_1 + \Phi_2 = \frac{1 - f + \beta f}{\alpha + 1 - f + \beta f} \quad (7)$$

Note that if $\beta = 1$, Φ_{1+2} does not depend on *f*.

The absorption cross section σ of the single crystal was obtained from the relationship between the initial absorbance and the crystal thickness (Supporting Information), yielding σ(405 nm) = 1.5×10^{-17} cm^2 molecule^{-1}. In order to assess the generality and robustness of the results, the time-dependent absorption curves of multiple single crystals and polycrystalline films were measured. The results described below are for three single crystals (samples 1–3) and three polycrystalline films (samples 4–6). Figures 2b and 2c showed the absorption spectra and the decay of sample 1, while the results for sample 4 are shown in Figure 2d. The evolution of the quantum yields as a function of *f* is shown in Figures 2e and 2f. The results are summarized in Table 1.

Table 1. Summary of the constants obtained by fitting.

	Sample number	α	β	$\Phi_{1,\,f=0}$	$\Phi_{2,\,f=0}$	$\Phi_{1,\,f=1}$	$\Phi_{2,\,f=1}$	$\frac{\Phi_{1+2,\,f=1}}{\Phi_{1+2,\,f=0}}$
Single Crystal	1	1.7	14	0.37	0.0	0.0	0.89	2.4
	2	0.90	53	0.53	0.0	0.0	0.98	1.9
	3	2.4	82	0.30	0.0	0.0	0.97	3.3
Polycrystalline film[a]	4	13	24	0.073	0.0	0.0	0.65	8.9
	5	10	9.6	0.090	0.0	0.0	0.49	5.4
	6	11	14	0.085	0.0	0.0	0.57	6.7

[a] σ was set to 3.0×10^{-17} cm^2 molecule^{-1}.

Simulations using Equation (5) (Supporting Information) demonstrated that $\frac{\Phi_{1+2,\,f=1}}{\Phi_{1+2,\,f=0}}$ was a useful quantity to parameterize the decay shape. With the relatively large ratio, the curves have a definite induction period. On the other hand, as the ratio approaches unity, the curves are closer to single-exponential because in this limit the total quantum yield is constant over the entire course of the reaction. $\frac{\Phi_{1+2,\,f=1}}{\Phi_{1+2,\,f=0}}$ was in the range 1.9–3.3 for single crystals and 5.4–8.9 for polycrystalline films. This is consistent with the different curve shapes in Figures 2c and 2d. This difference is mostly caused by the initial Φ_1. $\Phi_{1,\,f=0}$ in a single crystal is about 5 times larger than in polycrystalline film. Note that this holds for any value of σ in the range 2.0×10^{-17}–8.0×10^{-17} cm^2 molecule^{-1}, so it does not rely on the exact value of the absorption cross-section, which has some uncertainty.

From Table 1, we see that Φ_{1+2} changes much more for the polycrystalline film than for the single crystal. This is due to a low $\Phi_{1,\,f=0}$ value for the polycrystalline film, since at high *f*

values the total quantum yields become similar. It appears that the reaction in the polycrystalline film benefits strongly from the presence of more B photodimers. Although we cannot determine the exact physical origin of this difference between **9MA** crystal morphologies, we can advance a hypothesis. **9MA** polycrystalline films presumably have higher defect densities than **9MA** single crystals. Singlet excitons in **9MA** polycrystalline film are likely to diffuse to defect sites which can lead to relaxation without photoreaction, accounting for the lower $\Phi_{1+2,\,f\,=\,0}$. Eventually, the defect sites will react and become photodimer domains, effectively removing them as trap sites. As the reaction proceeds, the defective polycrystalline film effectively anneals itself and the excited states created at high *f* values experience a high quantum yield as the trapping deactivation pathway is removed. For high quality single crystals with fewer defect sites, on the other hand, the competing defect site relaxation channel will be negligible for both small and large *f* values. Slight differences in the reaction quantum yields in each group of single crystals (samples 1–3) and polycrystalline films (samples 4–6) may be attributed to different defect densities. Interestingly, the ratio $\frac{\Phi_{1+2,\,f\,=1}}{\Phi_{1+2,\,f\,=0}}$ does not approach unity for any of the single crystal samples. One explanation is that there are enough defects even in the single crystal to suppress the initial quantum yield, albeit much less than in the polycrystalline films. A second possibility is that the geometrical change associated with dimerization leads to changes in the crystal environment of the remaining monomer pairs, for example forcing them closer together and thus facilitating their dimerization. Distinguishing between the roles played by defects and intrinsic crystal structure changes in the overall photochemical reaction rate will require detailed crystal characterization and more sophisticated theoretical models. We emphasize that the kinetic model presented here provides one possible way to parameterize the nonstationary kinetics **9MA**, and there may be other models

that can also describe the phenomenon. The important point is that crystal quality appears to play an important role in giving rise to the sigmoidal reaction kinetics.

The fact that the kinetics in **9MA** single crystals are closer to single-exponential provides a hint that the reaction takes place homogeneously across the crystal. To confirm this, we have performed two types of measurements to spatially resolve the reaction progress within a single crystal. First, the time-dependent birefringence was investigated. We have reported photoinduced interference color change accompanying birefringence change of diarylethene single crystal.[45,46] The interference color change and birefringence change are very sensitive to the photoreaction in single crystal. To spatially track the photoreaction in single crystal, birefringence is a very useful method. If the transformation mechanism of **9MA** crystals is martensitic, the interference color should change following a well-defined phase front that propagates across the crystal, as seen for thermally induced martensitic transitions.[36] Before the change in the interference color was investigated in detail, the changes in the optic axes between the initial crystal and the completely reacted crystal were measured. If the optic axes change before and after the photoreaction, a more complex analysis considering the optic axes change would be required. The optic axes with a sensitive-tint plate and a 1/4 wavelength plate are shown in Figures S12 and S13. The birefringence was confirmed even after completion of the photoreaction, which indicated that the crystal state was maintained during the transformation. Moreover, the optic axes did not change, indicating that the herringbone molecular packing motif that determines the optic axes in **9MA** crystals did not change during the photoreaction.

After determination of the optic axes, the change in interference color of the crystals accompanying the photodimerization reaction upon irradiation with UV light was investigated. A **9MA** crystal with a thickness of 1.5 μm appeared orange under crossed Nicols as shown in Movie

S1 and Figure 3a. Upon UV irradiation at 405 nm, the interference color uniformly changed from orange to pale orange, yellow, pale yellow, and white over the whole crystal. Even in crystals with high aspect ratios, the interference color homogeneously changed over the whole crystal as shown in Movie S2 and Figure S14. To quantitatively evaluate the interference change, the birefringence (Δn) change was measured by Sénarmont method as shown in Figure 3b. The initial value was about 0.29 and then gradually decreased to about 0.18 after 120 seconds of UV irradiation. The dynamic change in the birefringence showed only a small amount of sigmoidal behavior, similar to the absorption change in single crystals. When the absorption spectra and birefringence values were measured at the same time, the relationship between the dimer fraction and the birefringence could be determined as shown in Figure S17b. There were some experimental outliers, but the relationship indicated the linear curve, which obviously demonstrated that the birefringence changed accompanying the photodimerization of **9MA**. The decrease in Δn could be reproduced by quantum chemical calculations of the molecular polarizability anisotropy change (Supporting Information). Thus, the evolution of the birefringence signal reflects a change in molecular electronic properties rather than crystal orientation or thickness.

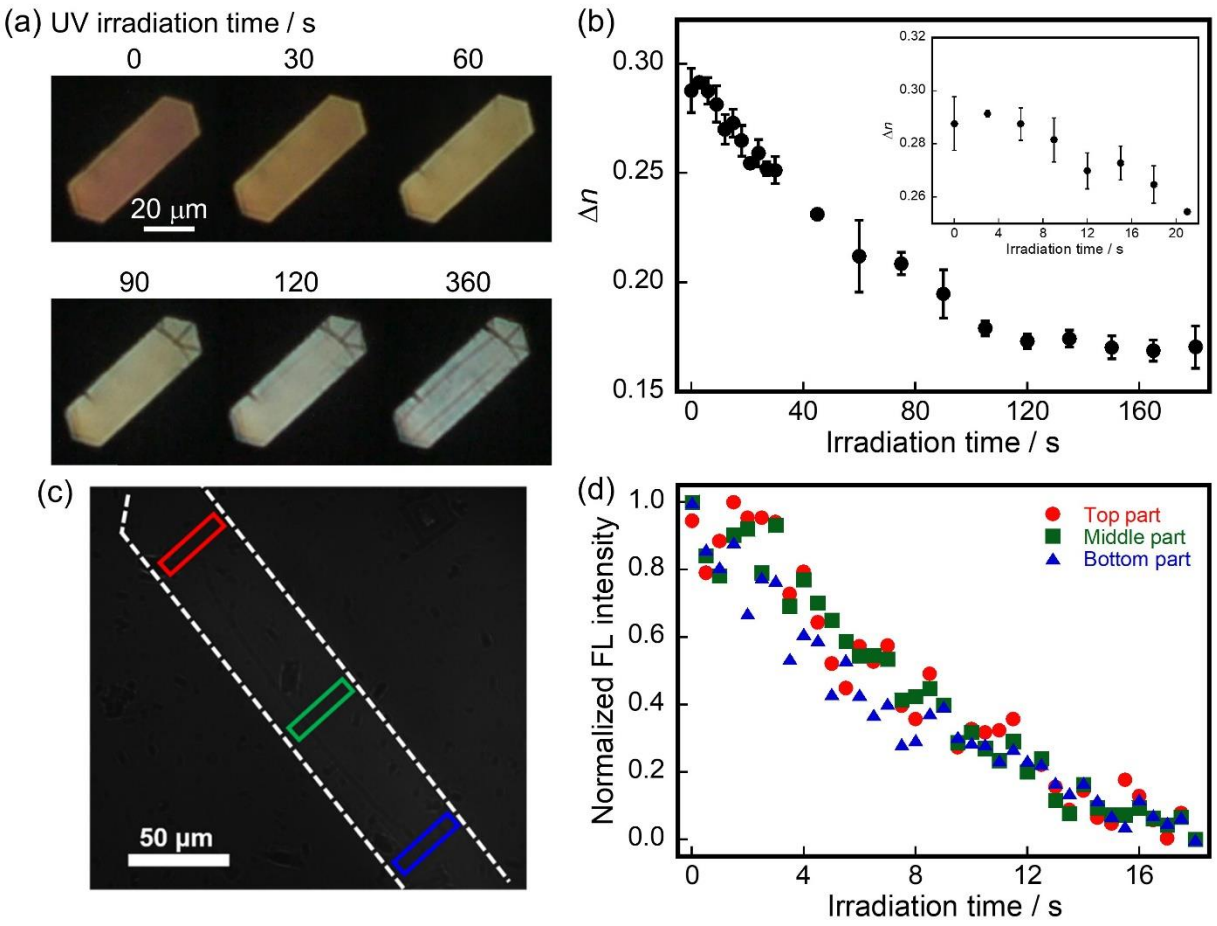

Figure 3. (a) Interference color change of **9MA** crystal with 1.5 μm of the thickness under crossed Nicols was observed by irradiated 365 nm. The irradiated power is 1.5 mW cm^{-2}. (b) Birefringence change with 0.7 μm of the thickness was measured. The wavelength and the power of the irradiated light for the dimerization reaction was 405 nm and 1.6 mW cm^{-2}, respectively. (c) Fluorescence optical microscope image of the single **9MA** microcrystal under 365 nm light irradiation (1.5 mW cm^{-2}) that was used for spatial fluorescence measurements. (d) The evolution of the 500 nm fluorescence output of the single **9MA** crystal from (c) during 365 nm irradiation. The colors of data points are associated with the regions that are labeled in (c).

The spatially homogeneous transformation of the **9MA** crystals was confirmed by a second set of spatially resolved fluorescence measurements on single crystals. We show the evolution of the 500 nm fluorescence output of a single **9MA** crystal during 365 nm irradiation as shown in Figure 3c. The overall brightness decreases uniformly across the crystal. In the image, we mark 3

separate regions of the crystal and we overlay the decay of the excimer fluorescence signal for each region (Figure 3d). The time-dependent decays, which reflect the disappearance of the monomer, overlap closely, again showing that the photodimerization reaction proceeds uniformly across the crystal.

Photomechanical response.

Given that the photochemical reaction occurs homogeneously (at least on optical lengthscales), the next question is how the molecular reaction dynamics are linked to the mechanical response. When exposed to UV light, the **9MA** crystals did not coil or bend but instead expanded in two different modes. About 90% of the dry and sandwiched crystals underwent a smooth expansion along the *c*-axis and contraction along the *b*-axis, as illustrated in Figure 4 and Movie S3. This dimensional change was sometimes accompanied by the development of isolated cracks that propagated at right angles to the crystal axes, but the overall crystal shape was always maintained. In rare (<10%) cases, the sandwiched crystals exhibited a radically different response. During illumination, the crystal would begin expanding but then suddenly explode into multiple random fragments. This sequence of events is illustrated in Figure 5 and Movie S4. Previous atomic force microscopy experiments on **9MA** crystals revealed dramatic surface morphology changes during photodimerization, [47] but we did not observe any increase in optical scattering that would correspond to such changes.

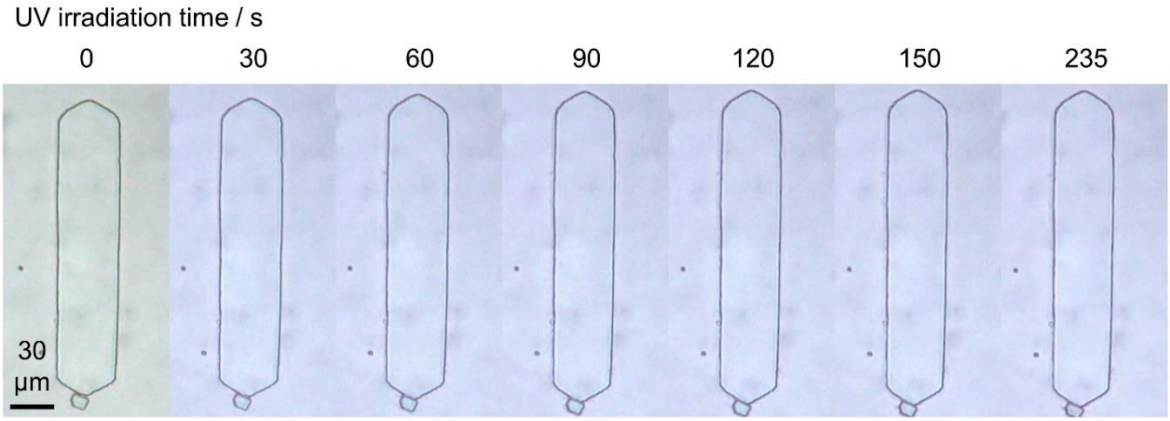

Figure 4. Dynamic crystal shape change of sample 7 upon UV irradiation. The wavelength and the power of the irradiated light for the dimerization reaction was 405 nm and 1.6 mW cm^{-2}, respectively.

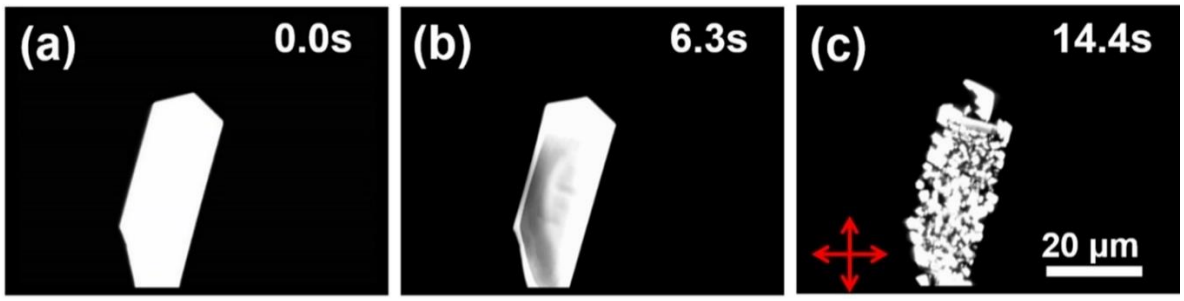

Figure 5. Sequential cross-polarized microscope images of **9MA** microcrystal showing exploding under 405 nm light irradiation (1.75 mW cm^{-2}) when clamped tightly between two glass slides. The red-cross indicates the direction of polarizer and analyzer (Movie S4).

The majority of crystals remain intact, and after complete photodimerization, the length increased by about 7% and the width decreased by about 4% as shown in Figure 6a. To confirm reproducibility, additional crystals (samples 8–11) were observed (Movies S5–S8). The time required to attain the final crystal size was on the order of 4 minutes under these conditions. All the samples exhibited a length increase of about 7% and a width decrease of about 4% (Figure 6). The length and the width of our **9MA** crystal plates correspond to the *c*-axis and the *b*-axis in the

unit cell of **9MA** crystal, respectively. The observed changes in crystal size can be directly inferred from changes in the unit cell parameters reported in 2003 by Turowska-Tyrk *et al*. using single crystal X-ray diffraction.[43] If that data for partially converted single crystals is extrapolated to 100% conversion, it predicts an expansion along the *c*-axis of 6.3% and a contraction along the *b*-axis of 3.0% as shown in Figure S21. The values are in very good agreement with our measured values for the length and width for 100% conversion as obtained from the data in Figure 6, consistent with a crystal-to-crystal transformation of **9MA** that proceeds smoothly all the way to 100% conversion.

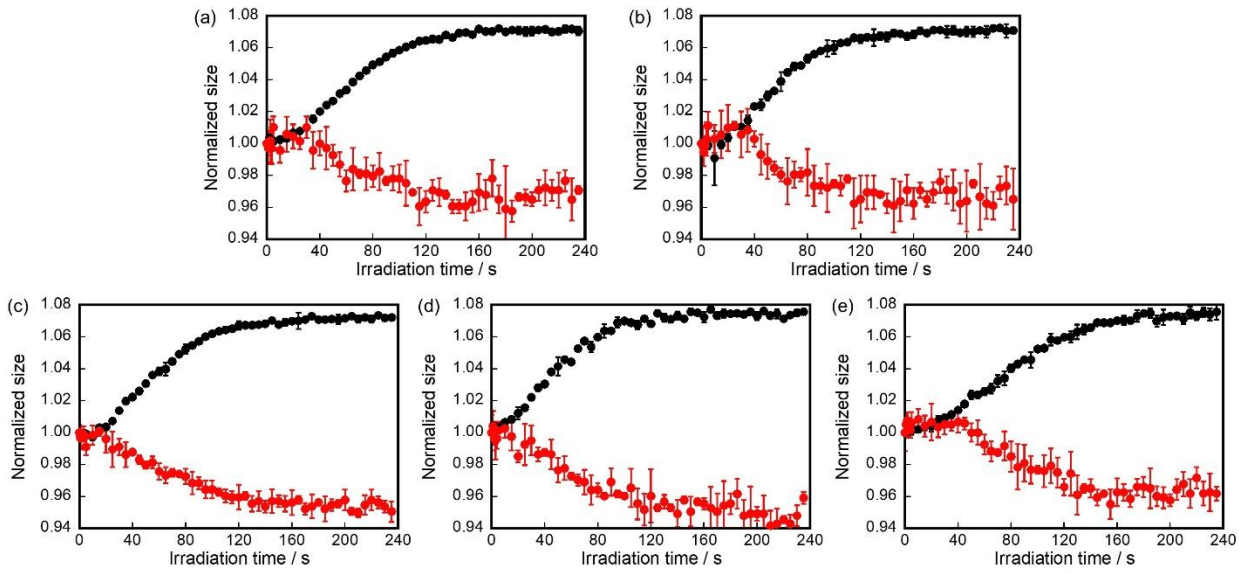

Figure 6. (a) sample 7, (b) sample 8, (c) sample 9, (d) sample 10, and (e) sample 11. The wavelength and the power of the irradiated light for the dimerization reaction was 405 nm and 1.6 mW cm^{-2}, respectively.

To correlate the reaction dynamics with the crystal expansion, we simultaneously measured the absorption and size changes of single crystals under 405 nm illumination. Except for the

exploding crystals, the ability of the plates to retain their overall shape and orientation allowed their optical properties to be probed during the mechanical response. The change in length ΔL tracked the loss of monomer absorption, and thus the photodimer population. The fraction of crystal converted to photodimer is given by

$$f = 1 - Abs' \qquad (8)$$

where *Abs'* is the absorbance of the monomer, integrated from 400–450 nm and normalized to the value before irradiation. The relation between ΔL, the expansion along the *c*-axis, and *f* is plotted in Figure 7 for three different crystal samples. The dependence of ΔL on *f* over almost the entire range shows that $\Delta L \propto f$. The fact that the dimensional change mirrors the reaction progress makes this crystal expansion well-behaved in the sense that there is no evidence of sudden transitions or strain build-up and release, as observed in photosalient crystals. Again, this homogeneous behavior could be a consequence of using high quality single crystals with a relatively low defect density. This observation also helps explain the "explosion" seen in Figure 5. Homogeneous strain build-up throughout the crystal can be released by fracture instead of expansion, but this has to occur simultaneously at all points, rather than at an isolated line of high stress at a reactant-product interface.

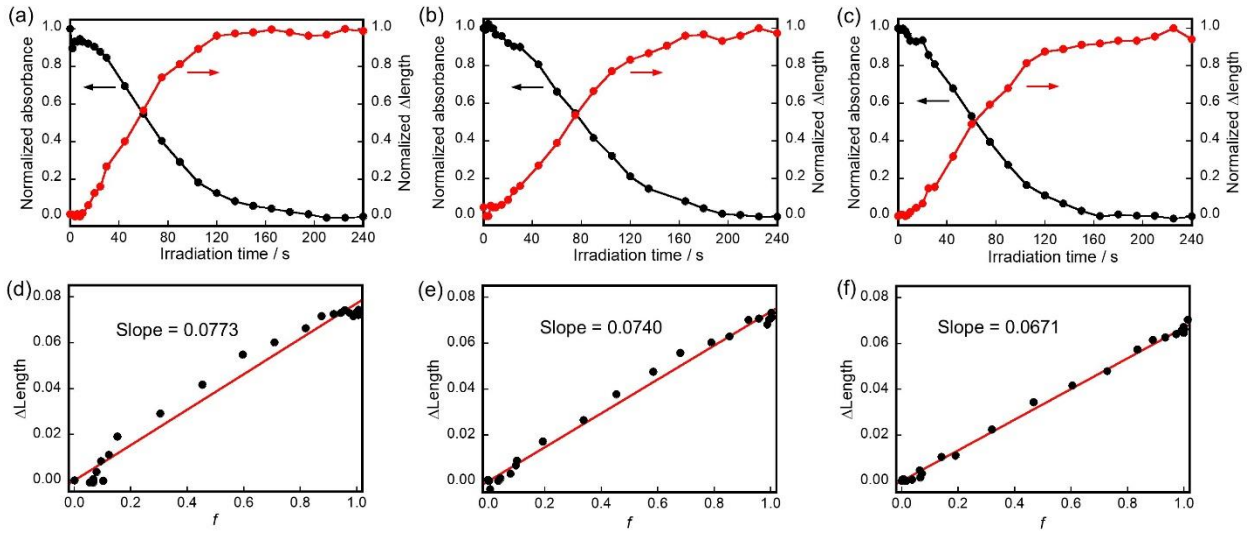

Figure 7. Normalized absorbance and length change of (a) sample 12, (b) sample 13, and (c) sample 14. The wavelength and the power of the irradiated light for the dimerization reaction was 405 nm and 1.6 mW cm^{-2}, respectively. The relationships between the dimer fraction and the length of (d) sample 12, (e) sample 13, and (f) sample 14 were shown.

It is important to note that the expanded unit cell obtained extrapolating from the expanded monomer unit cell does not correspond to the crystal structure of the photodimer grown from solution as previously noted by Turowska-Tyrk.[43,48] It seems that solid-state dimerization leads to a different dimer crystal polymorph, as observed in other anthracene derivatives.[49] In the Supporting Information, we present solid-state NMR data that is consistent with this possibility, but since the current paper focuses on the reaction dynamics, detailed characterization of the crystal produced by solid-state photodimerization must be reserved for future work. Eventually, the quantitative prediction of the crystal expansion/contraction will require precise determination of this crystal packing and orientation.

Overall, the data show that a single-crystal-to-single-crystal transformation can occur in a homogeneous, predictable manner without sudden jumps or phase separation. The picture that emerges is that high-quality **9MA** single crystals have a relatively simple reaction path in which

the photodimer and monomer form a solid solution with a crystal lattice that changes smoothly with increasing dimer concentration, basically following Vegard's Law for a solid solution.[50–52] There is no sign of heterogeneous phase separation on optical lengthscales. Both the reaction dependent quantum yields and the correlation between reaction progress and expansion should be present for any light intensity according to our model. It is possible that very high light intensities could drive the photodimerization to completion before the physical expansion occurs, causing the correlation to break down, but this regime would require high energy laser excitation and is beyond the scope of this work. The physical explanation for **9MA**'s homogeneous behavior may lie in the relatively weak Van der Waals forces between the dimer pairs. If photodimerization does not lead to large changes in the intermolecular interaction energies, there is no energetic benefit for nucleation of phase separation. It would be interesting to examine the same reaction in a crystal with strong intermolecular interactions, e.g. hydrogen bonds, to see whether any signatures of a martensitic photomechanical phase transition could be observed. It would also be desirable to perform these measurements on a crystal where the photochemistry can be completely reversed, in order to confirm that the size change could be reversed as well. Assuming that mechanical fatigue (cracking, defect creation) can be avoided during this cycling, a fully reversible photochemical system could provide the basis for a practical actuator.

Conclusions

The dynamic photoinduced shape change of crystalline **9MA** during photochemical reaction has been characterized in this work. Remarkably, the photochemical kinetics depend on crystal morphology, with single crystals approaching single-exponential behavior while polycrystalline films have a pronounced sigmoidal character. We develop a new kinetic model that can describe both regimes in terms of an effective quantum yield that depends on reaction progress. Differences in the behavior of single crystals versus crystalline powders are rationalized in terms of different structural defect densities in the two types of samples, combined with the loss of defective sites as the reaction proceeds. The simpler kinetics in single crystals are accompanied by a reproducible expansion along the *c*-axis and contraction along the *b*-axis. As long as the crystals are relatively thin (< 1 μm), this shape change occurs homogeneously across the crystal. Time-resolved birefringence and fluorescence measurements on single crystals are consistent with spatially homogeneous mixing of the monomer reactant and photodimer product. This uniform strain leads to a novel photoinduced crystal explosion in some cases, but in most cases it leads to a smooth shape transition where the lattice parameters change in parallel to the photochemical reaction progress.

The results in this paper demonstrate that a single molecular crystal can undergo a 100% phase change driven by photochemistry. It should be possible to harness these well-defined, reproducible expansions for light-powered actuation, in contrast to the bending motions usually observed. A necessary condition for these observations is the growth of loosely bound high-quality single crystals, and we hope our results motivate future work on reversible negative photochromic reactions that can occur in crystal environments.

Experimental Section

Detailed descriptions of materials, microscopic observation of crystals, and fluorescence measurements can be found in the Supporting Information.

Acknowledgments.

This work was supported by JSPS KAKENHI Grant Numbers 20J20030 (K.M.), 21K14603 (D.K.), 21H02016 (S.K.), and the Office of Naval Research through the MURI on Photomechanical Material Systems (ONR N00014-18-1-2624) (C.J.B.).

Keywords

kinetics, organic crystal, phase transition, photochemistry, photomechanical actuator

Present Address.

Present address for F.T: Key Laboratory for Advanced Materials and Joint International Research Laboratory of Precision Chemistry and Molecular Engineering, Feringa Nobel Prize Scientist Joint Research Center, Frontiers Science Center for Materiobiology and Dynamic Chemistry, Institute of Fine Chemicals, School of Chemistry and Molecular Engineering, East China University of Science and Technology, Shanghai, 200237 China

References.

[1] *Photomechanical Materials, Composites, and Systems: Wireless Transduction of Light into Work*, (Eds.: T. J. White), Wiley, Hoboken, **2017**.

[2] *Mechanically Responsive Materials for Soft Robotics*, (Eds.: H. Koshima), Wiley, Weinheim, **2019**.

[3] P. Naumov, S. Chizhik, M. K. Panda, N. K. Nath, E. Boldyreva, *Chem. Rev.* **2015**, *115*, 12440–12490.

[4] R. O. Al-Kaysi, C. J. Bardeen, *Adv. Mater.* **2007**, *19*, 1276–1280.

[5] S. Kobatake, S. Takami, H. Muto, T. Ishikawa, M. Irie, *Nature* **2007**, *446*, 778–781.

[6] H. Koshima, N. Ojima, H. Uchimoto, *J. Am. Chem. Soc.* **2009**, *131*, 6890–6891.

[7] O. S. Bushuyev, A. Tomberg, T. Friščić, C. J. Barrett, *J. Am. Chem. Soc.* **2013**, *135*, 12556–12559.

[8] R. Nishimura, A. Fujimoto, N. Yasuda, M. Morimoto, T. Nagasaka, H. Sotome, S. Ito, H. Miyasaka, S. Yokojima, S. Nakamura, B. L. Feringa, K. Uchida, *Angew. Chem. Int. Ed.* **2019**, *58*, 13308–13312; *Angew. Chem.* **2019**, *131*, 13442–13446.

[9] L. Zhu, R. O. Al-Kaysi, C. J. Bardeen, *J. Am. Chem. Soc.* **2011**, *133*, 12569–12575.

[10] D. Kitagawa, H. Nishi, S. Kobatake, *Angew. Chem. Int. Ed.* **2013**, *52*, 9320–9322; *Angew. Chem.* **2013**, *125*, 9490–9492.

[11] T. Kim, M. K. Al-Muhanna, S. D. Al-Suwaidan, R. O. Al-Kaysi, C. J. Bardeen, *Angew. Chem. Int. Ed.* **2013**, *52*, 6889–6893; *Angew. Chem.* **2013**, *125*, 7027–7031.

[12] J. M. Cole, J. de J. Velazquez-Garcia, D. J. Gosztola, S. G. Wang, Y.-S. Chen, *Chem. Mater.* **2019**, *31*, 4927–4935.

[13] F. Tong, M. Al-Haidar, L. Zhu, R. O. Al-Kaysi, C. J. Bardeen, *Chem. Commun.* **2019**, *55*, 3709–3712.

[14] M. Tamaoki, D. Kitagawa, S. Kobatake, *Cryst. Growth Des.* **2021**, *21*, 3093–3099.

[15] P. Naumov, S. C. Sahoo, B. A. Zakharov, E. V. Boldyreva, *Angew. Chem. Int. Ed.* **2013**, *52*, 9990–9995; *Angew. Chem.* **2013**, *125*, 10174–10179.

[16] E. Hatano, M. Morimoto, T. Imai, K. Hyodo, A. Fujimoto, R. Nishimura, A. Sekine, N. Yasuda, S. Yokojima, S. Nakamura, K. Uchida, *Angew. Chem. Int. Ed.* **2017**, *56*, 12576–12580; *Angew. Chem.* **2017**, *129*, 12750–12754.

[17] D. Kitagawa, S. Kobatake, *J. Phys. Chem. C* **2013**, *117*, 20887–20892.

[18] T. Kim, L. Zhu, L. J. Mueller, C. J. Bardeen, *J. Am. Chem. Soc.* **2014**, *136*, 6617–6625.

[19] N. K. Nath, L. Pejov, S. M. Nichols, C. Hu, N. Saleh, B. Kahr, P. Naumov, *J. Am. Chem. Soc.* **2014**, *136*, 2757–2766.

[20] G. Liu, J. Liu, Y. Liu, X. Tao, *J. Am. Chem. Soc.* **2014**, *136*, 590–593.

[21] M. K. Panda, T. Runčevski, S. Chandra Sahoo, A. A. Belik, N. K. Nath, R. E. Dinnebier, P. Naumov, *Nat. Commun.* **2014**, *5*, 4811.

[22] *Photochromism: Molecules and Systems*, (Ed.: H. Durr, H. Bouas-Laurent), Elsevier, Amsterdam, **2003**.

[23] S. Aiken, R. J. L. Edgar, C. D. Gabbutt, B. M. Heron, P. A. Hobson, *Dyes Pigments* **2018**, *149*, 92–121.

[24] A. E. Keating, M. A. Garcia-Garibay in *Organic and Inorganic Photochemistry*, Vol. 2 (Eds.: V. Ramamurthy, K. S. Schanze), Marcel Dekker, New York, **1998**, pp. 195–248.

[25] S. Takahashi, H. Miura, H. Kasai, S. Okada, H. Oikawa, H. Nakanishi, *J. Am. Chem. Soc.* **2002**, *124*, 10944–10945.

[26] R. O. Al-Kaysi, A. M. Müller, C. J. Bardeen, *J. Am. Chem. Soc.* **2006**, *128*, 15938–15939.
[27] D.-K. Bučar, L. R. MacGillivray, *J. Am. Chem. Soc.* **2007**, *129*, 32–33.
[28] M. Bertmer, R. C. Nieuwendaal, A. B. Barnes, S. E. Hayes, *J. Phys. Chem. B* **2006**, *110*, 6270–6273.
[29] J. Davaasambuu, G. Busse, S. Techert, *J. Phys. Chem. A* **2006**, *110*, 3261–3265.
[30] J. D. Dunitz, *Pure Appl. Chem.* **1991**, *63*, 177–185.
[31] J. W. Christian, G. B. Olson, M. Cohen, *J. Phys. IV* **1995**, *05*, C8–3–C8–10.
[32] *The Theory of Transformations in Metals and Alloys*, (Ed.: J. W. Christian), Pergamon, Oxford, **2002**.
[33] S. K. Park, Y. Diao, *Chem. Soc. Rev.* **2020**, *49*, 8287–8314.
[34] O. Scheidsteger, G. Huttner, V. Bejenke, W. Gartzke, *Z. Für Naturforschung B* **1983**, *38*, 1598–1614.
[35] M. T. Ruggiero, J. A. Zeitler, T. M. Korter, *Phys. Chem. Chem. Phys.* **2017**, *19*, 28502–28506.
[36] H. Chung, D. Dudenko, F. Zhang, G. D'Avino, C. Ruzié, A. Richard, G. Schweicher, J. Cornil, D. Beljonne, Y. Geerts, Y. Diao, *Nat. Commun.* **2018**, *9*, 278.
[37] S. W. Kennedy, *J. Mater. Sci.* **1974**, *9*, 1391–1392.
[38] Yu. V. Mnyukh, N. A. Panfilova, N. N. Petropavlov, N. S. Uchvatova, *J. Phys. Chem. Solids* **1975**, *36*, 127–144.
[39] S. Yamamoto, K.-H. Grellmann, A. Weller, *Chem. Phys. Lett.* **1980**, *70*, 241–245.
[40] E.-Z. M. Ebeid, A.-F. M. Habib, S. A. Azim, *React. Solids* **1988**, *6*, 39–44.
[41] A. S. Dvornikov, P. M. Rentzepis, *Res. Chem. Intermed.* **1996**, *22*, 115–128.
[42] F. Tong, W. Xu, M. Al‐Haidar, D. Kitagawa, R. O. Al‐Kaysi, C. J. Bardeen, *Angew. Chem. Int. Ed.* **2018**, *57*, 7080–7084; *Angew. Chem.* **2018**, *130*, 7198–7202.
[43] I. Turowska-Tyrk, E. Trzop, *Acta Crystallogr. Sect. B* **2003**, *59*, 779–786.
[44] F. Tong, M. P. Hanson, C. J. Bardeen, *Phys. Chem. Chem. Phys.* **2016**, *18*, 31936–31945.
[45] K. Morimoto, H. Tsujioka, D. Kitagawa, S. Kobatake, *Bull. Chem. Soc. Jpn.* **2019**, *92*, 1299–1304.
[46] K. Morimoto, H. Tsujioka, D. Kitagawa, S. Kobatake, *J. Phys. Chem. A* **2020**, *124*, 4732–4741.
[47] G. Kaupp, *Angew. Chem. Int. Ed. Engl.* **1992**, *31*, 595–598; *Angew. Chem.* **1992**, *104*, 609–612.
[48] J. C. J. Bart, G. M. J. Schmidt, *Isr. J. Chem.* **1971**, *9*, 429–448.
[49] K. R. Chalek, X. Dong, F. Tong, R. A. Kudla, L. Zhu, A. D. Gill, W. Xu, C. Yang, J. D. Hartman, A. Magalhães, R. O. Al-Kaysi, R. C. Hayward, R. J. Hooley, G. J. O. Beran, C. J. Bardeen, L. J. Mueller, *Chem. Sci.* **2021**, *12*, 453–463.
[50] D. L. Dorset, W. A. Pangborn, *Proc. Natl. Acad. Sci.* **1992**, *89*, 1822–1826.
[51] H. H.-M. Yeung, W. Li, P. J. Saines, T. K. J. Köster, C. P. Grey, A. K. Cheetham, *Angew. Chem. Int. Ed.* **2013**, *52*, 5544–5547; *Angew. Chem.* **2013**, *125*, 5654–5657.
[52] S. P. Thomas, R. Sathishkumar, T. N. G. Row, *Chem. Commun.* **2015**, *51*, 14255–14258.

Table of contents

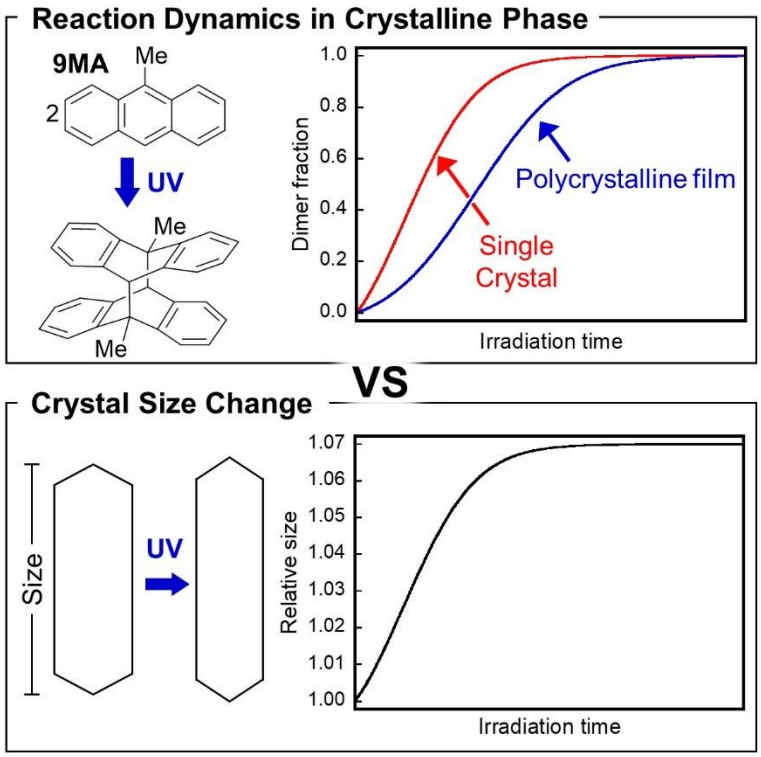

The development of a nonlinear kinetic model for crystal reactions allows us to quantify for the first time how the kinetics depend on sample morphology. And the quantitative connection between molecular reaction kinetics and mechanical response in well-defined single crystals provides a new benchmark for analyzing these photomechanical materials.